The Influence of Deviation from Circularity on the Stress of a Pressurized Fuel Cylindrical Tank

Assoc. Prof. PhD. Eng. **Ștefan ŢĂLU**[1], Assoc. Prof. PhD. Eng. **Mihai ŢĂLU**[2,*]

[1] Technical University of Cluj-Napoca, The Directorate of Research, Development and Innovation Management (DMCDI), Constantin Daicoviciu Street, no. 15, Cluj-Napoca, 400020, Cluj county, Romania. E-mail: stefan_ta@yahoo.com

[2] University of Craiova, Faculty of Mechanics, Department of Applied Mechanics and Civil Engineering, Calea București Street, no. 107, 200512 Craiova, Dolj county, Romania. Corresponding author* e-mail: mihai_talu@yahoo.com

§: Both authors contributed equally to this work.

Abstract: *The objective of this study is to determine the state of stress that occurs in the shape deformation of the lateral shell of a pressurized fuel cylindrical tank made of AISI 4340 steel, by modification of the cylindrical shape to an elliptical shape. The study of the state of efforts is carried out in the context of the overlapping of the influence of the deviations of the form over the influences caused by the temperature and corrosion variation. The CAD analysis is done on a parameterized model, finalizing with the determination of the laws of variation of the stress by polynomial interpolation and graphical representation. In this study it is also defined the graphic domain characterized by parameters such as: temperature T, pressure p, duration of exploitation and coefficient of ellipticity k, for which the lateral is oved from use as a result of exceeding the admissible effort values.*

Keywords: *Automotive industry, coefficient of ellipticity, corrosion, elliptical cover, industrial engineering design, optimization methods, pressurized fuel tank*

1. Introduction

The fuel tanks market in the automotive industry has a dynamic development, sustained by the continuous research of trained specialists with direct applicability and utilization of high technologies [1-4]. These challenges help to increase safety in exploitation and competitiveness in production [5-9].
The construction geometry of pressurized fuel tanks (made especially of steel or aluminum) in the automotive industry is a complex process based on an appropriate documentation [10-13].
Pressurized cylindrical fuel tanks are used to store liquefied petroleum gas (LPG) or compressed natural gas (CNG) fuel. For these tanks the state of stress in the lateral cover has significant changes if there are circular deviations from the cylindrical shape [6]. On the other hand, other factors that influence the state of effort are: pressure, temperature and corrosion [7-10, 14, 15].
The hydraulic testing pressure of the pressurized fuel tank are relatively high and can attain up to a p = 300 bar in the case of CNG tanks [5, 6, 16]. The optimal engineering design of the fuel tanks, with more and less components, involves engineering level tools [17-28], both computational and experimental, which includes modeling [29-37] and testing to a better solution at less cost [38-44].
In practice, the transformation of the lateral cover of a cylindrical fuel tank into an elliptical shape can be found either by the inappropriate application of some technological processes in the realization of the covering or as a result of an impact resulting from a road accident.

2. The parameterized model of the elliptical lateral cover of the pressurized fuel tank

This study was performed on an optimally designed lateral cover of a pressurized cylindrical fuel tank, which was deformed into an elliptical shape. The cylindrical initial shape of the lateral cover and its state of stress constitute the basis of comparison of the effect introduced on the state of stress by deforming it in elliptical form. The parametric modeling of the pressurized cylindrical fuel tank was made with AutoCAD Autodesk 2017 software [45].
The initial data of design process for the cylindrical lateral cover are:
- maximum hydraulic test pressure p_{max} = 30 N/mm^2; on the interior surface S_5, (Figure 1);

- working temperature with variation between the limits T = -30 ^{0}C up to T = +60 ^{0}C, on the exterior surface S_6, (Figure 1); - the corrosion velocity of the material: v_c = 0.12 mm/year;
- the lateral cover material, AISI 4340 steel; - the exploitation period: n_a = 20 years;
- the outer diameter and length of the lateral cover are: ϕ = 250 mm and L = 700 mm, (Figure 1).

Noting with: a and b, the semi-major and semi-minor axes of the ellipse, the coefficient of ellipticity k_e is given by the following formula:

$$k_e = \frac{a}{b} > 1 \tag{1}$$

It is assumed the medium perimeter of the initial ring section passing in the elliptical form is equal to the medium perimeter of the elliptical ring section after deformation, according next formula:

$$2\pi R = \frac{3\pi}{2}(a+b) - \pi\sqrt{a \cdot b} \tag{2}$$

If we take into account the calculation formula of the coefficient of ellipticity k_e, then the median annular ellipse semi-axes have the graphic variation given in Figure 2 and can be calculated with the following formulas:

$$b = \frac{4R}{3(k_e+1) - 2\sqrt{k_e}} \;;\; a = b \cdot k_e \tag{3}$$

Based on the symmetry of the lateral cover with respect to the planes containing the semi-major and semi-minor axes of ellipse and of the longitudinal axis of the lateral cover our study was carried out on a model divided into ½ of the initial shape of the lateral cover (Figure 1).

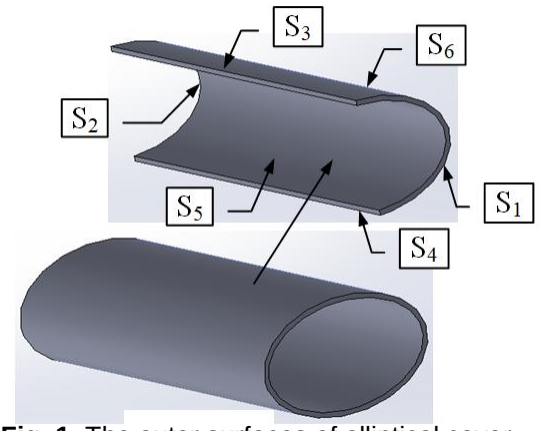

Fig. 1. The outer surfaces of elliptical cover

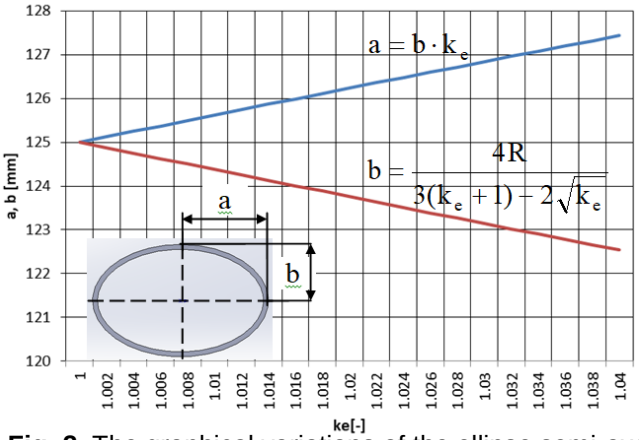

Fig. 2. The graphical variations of the ellipse semi-axes

3. The CAD study of the Von Mises stress state in the elliptical lateral cover

The existence of the two head cover with the pressure p_{max} = 30 N/mm^2 on the inner surfaces S_5, causes the apparition of two traction forces on the end surfaces: S_1 and S_2, Figure 1, which have the following value:

$$F = \pi a b p_{max} = \pi b^2 k_e p_{max} = \frac{16\pi R^2 k_e}{\left[3(k_e+1) - 2\sqrt{k_e}\right]^2} \cdot p_{max} = 1471875 \text{ N} \tag{4}$$

This model was imported to SolidWorks 2017 software [46] for analysis with the: Static, Thermal and Design Study modules. In this mode the variance of the Von Mises resultant stress on the lateral cover was calculated as a result of the requirements specified in the design data and the effect of the shape change in the cross-section through the coefficient of ellipticity.

The calculation was made for discrete values of: the coefficient of ellipticity, the thickness of the elliptical cover, the number of years of exploitation and the temperature variation.

The results are given in Tables 1 to 5. It is necessary to correctly evaluate the influence of ellipticity, take as base the Von Mises stress corresponding to the undeformed initial state of the lateral cover for k_e = 1, Table 1.

For each case of ellipticity, were calculated the laws of variation and plotted graphically [47, 48].

- the variation of the stress $\sigma(n_a, T = constant)$ and the laws of variation determined by polynomial interpolation, (as shown in Figure 3a to Figure 7a); the graph of the 3D variation of the stress dependence $\sigma\ (n_a, T)$, (as shown in Figure 3b to Figure 7b);
- the top view of the surface associated with the dependence $\sigma\ (n_a, T)$ on which the area delimited by temperature and years of exploitation can be identified, in which the cover loses its working capacity, being put out of use because the Von Mises stress exceeds the admitted effort of the material traction, $\sigma_a = 710\ N/mm^2$; (as shown in Figure 3c to Figure 7c);
- the graph of the percentage increase of the stress $\Delta\sigma\ (n_a, T = constant)$ for the elliptical shape, computed in relation to the undeformed initial state, on which identifies the maximum interval time from the beginning $n_{a\ maximum}$ of the maximum exploitation to which the covering is functional, specifying in the same time and the law of variation determined by an polynomial interpolation, (as shown in Figure 3d to Figure 7d);

For the initial cylindrical undeformed state of lateral cover the results are given in Table 1.

Table 1: The Von Mises stress in cylindrical lateral cover

	T [^{0}C]	-30^{0}C	-20^{0}C	-10^{0}C	0^{0}C	10^{0}C	20^{0}C	30^{0}C	40^{0}C	50^{0}C	60^{0}C
n_a [years]	**s [mm]**	**σ [N/mm^2]**									
0	9.2	531.36	504.46	478.19	453.75	431.69	410.54	395.55	398.56	406.94	417.27
1	9.08	533.07	506.18	480.48	455.45	434.48	414.31	400.03	404.09	413.49	424.81
2	8.96	535.17	508.31	483.13	459.47	437.6	418.34	404.76	409.77	420.13	432.35
3	8.84	537.67	510.85	486.15	462.83	441.05	422.65	409.74	415.6	426.85	439.91
4	8.72	540.57	513.81	489.54	466.53	444.84	427.21	414.95	421.57	433.64	447.48
5	8.6	543.87	517.17	493.3	470.55	448.96	432.05	420.41	427.7	440.52	455.06
6	8.48	547.54	520.95	497.42	474.91	453.41	437.15	426.12	433.98	447.48	462.64
7	8.36	551.66	525.15	501.91	479.6	458.19	442.52	432.06	440.41	454.53	470.24
8	8.24	556.15	529.75	506.77	484.63	463.31	448.15	438.26	446.98	461.65	477.84
9	8.12	561.05	534.77	512	489.99	468.76	454.05	444.69	453.71	468.85	485.46
10	8	566.33	540.2	517.59	495.68	474.55	460.22	451.37	460.58	476.13	493.09
11	7.88	572.02	546.04	523.56	501.7	480.66	466.65	458.29	467.61	483.5	500.72
12	7.76	578.11	552.29	529.89	508.06	487.11	473.35	465.46	474.79	490.94	508.37
13	7.64	584.59	558.96	536.58	514.75	493.9	480.31	472.87	482.11	498.47	516.02
14	7.52	591.47	566.04	543.65	521.78	501.01	487.54	480.53	489.54	506.08	523.68
15	7.4	598.75	573.53	551.08	529.13	508.46	495.04	488.42	497.21	513.77	531.36
16	7.28	606.42	581.44	558.88	536.82	516.24	502.81	496.57	504.98	521.54	539.04
17	7.16	614.5	589.75	567.05	544.85	524.36	510.84	504.95	512.91	529.39	546.73
18	7.04	622.97	598.48	575.58	553.21	532.81	519.14	513.58	520.98	537.32	554.44
19	6.92	631.85	607.62	584.49	561.9	541.59	527.7	522.45	529.21	545.33	562.15
20	6.8	641.11	617.18	593.76	570.92	550.7	536.53	531.57	537.58	553.42	569.87

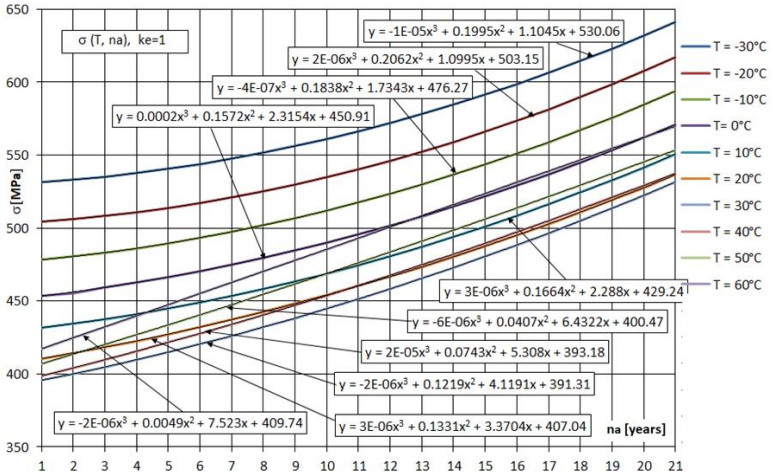

Fig. 3a. The graphs of Von Mises stress $\sigma\ (n_a, T = ct.)$ for $k_e = 1$

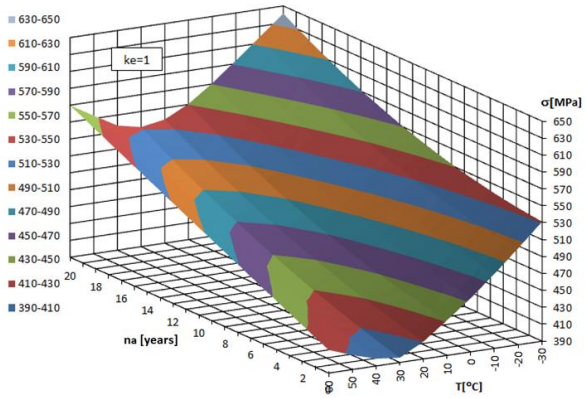

Fig. 3b. The graph of Von Mises stress σ (n_a,T) for k_e = 1

For lateral cover with ellipticity k_e = 1.01, the results are given in Table 2.

Table 2: The Von Mises stress in elliptical lateral cover with k_e = 1.01

	T [^{0}C]	-30^{0}C	-20^{0}C	-10^{0}C	0^{0}C	10^{0}C	20^{0}C	30^{0}C	40^{0}C	50^{0}C	60^{0}C
n_a [years]	s [mm]	σ [N/mm^2]									
0	9.2	592.96	565.46	540.59	517.38	494.84	474.26	459.46	445.65	443.25	450.76
1	9.08	600.32	572.31	546.50	522.74	499.90	478.77	464.03	450.84	448.48	456.04
2	8.96	607.34	579.06	552.48	528.22	505.11	483.54	468.87	456.27	453.89	461.46
3	8.84	614.64	585.75	558.50	533.81	510.50	488.56	473.96	461.90	459.47	467.03
4	8.72	621.6	592.4	564.58	539.52	516.06	493.82	479.30	467.74	465.22	472.74
5	8.6	628.44	598.99	570.70	545.35	521.80	499.34	484.89	473.79	471.14	478.59
6	8.48	635.14	605.53	576.88	551.3	527.71	505.11	490.73	480.04	477.23	484.59
7	8.36	641.71	612.02	583.11	557.37	533.79	511.12	496.82	486.50	483.5	490.73
8	8.24	648.16	618.45	589.39	563.56	540.05	517.39	503.16	493.16	489.94	497.01
9	8.12	654.47	624.84	595.71	569.86	546.48	523.91	509.75	500.03	496.55	503.44
10	8	660.63	631.16	602.1	576.3	553.05	530.75	516.16	507.12	503.33	509.97
11	7.88	666.7	637.45	608.53	582.83	559.86	537.69	523.67	514.39	510.28	516.73
12	7.76	672.62	643.67	615.01	589.49	566.82	544.95	531.00	521.89	517.41	523.59
13	7.64	678.41	649.85	621.54	596.27	573.94	552.46	538.59	529.58	524.71	530.59
14	7.52	684.07	655.97	628.13	603.17	581.24	560.23	546.42	537.49	532.18	537.74
15	7.4	689.6	662.04	634.76	610.19	588.71	568.24	554.51	545.60	539.82	545.04
16	7.28	0695	668.06	641.45	617.33	596.36	576.5	562.84	553.92	547.63	552.47
17	7.16	700.27	674.02	648.18	624.58	604.18	585.01	571.42	562.44	555.62	560.05
18	7.04	705.41	679.94	654.97	631.95	612.17	593.77	580.25	571.17	563.77	567.78
19	6.92	0	685.8	661.81	639.45	620.34	602.79	589.33	580.11	572.10	575.65
20	6.8	0	691.57	668.70	647.06	628.68	612.04	598.65	589.23	580.58	583.61

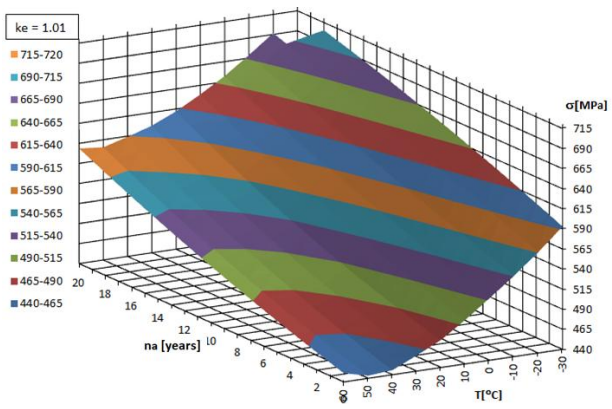

Fig. 4a. The graph of Von Mises stress σ (n_a,T) for k_e = 1.01

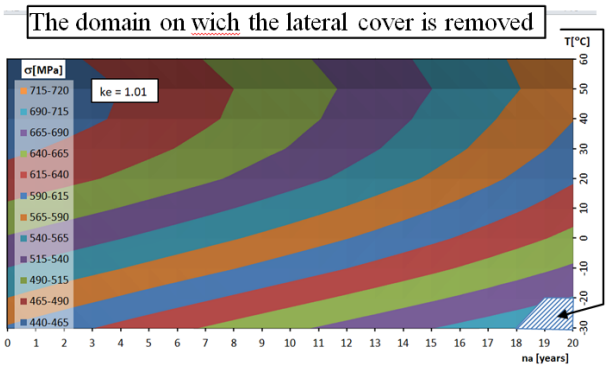

Fig. 4b. The graph in top view of Von Mises stress σ (n_a,T) for k_e = 1.01

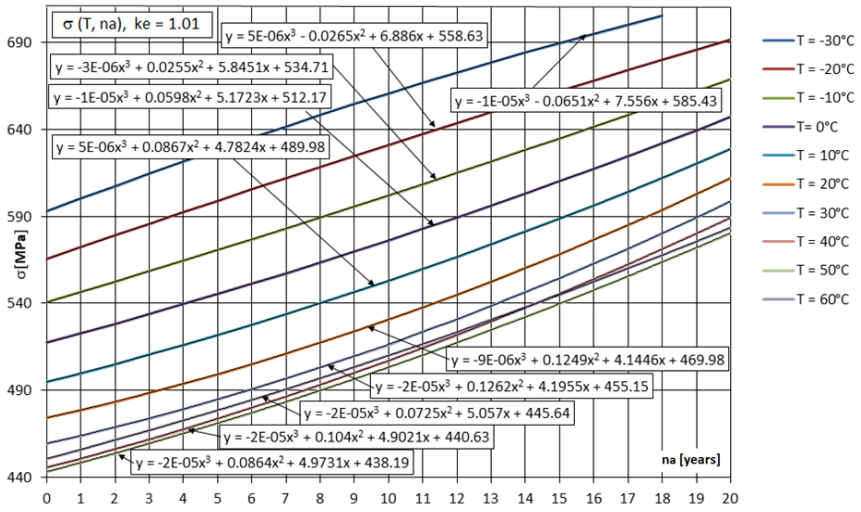

Fig. 4c. The graphs of Von Mises stress σ (n_a,T = ct.) for k_e = 1.01

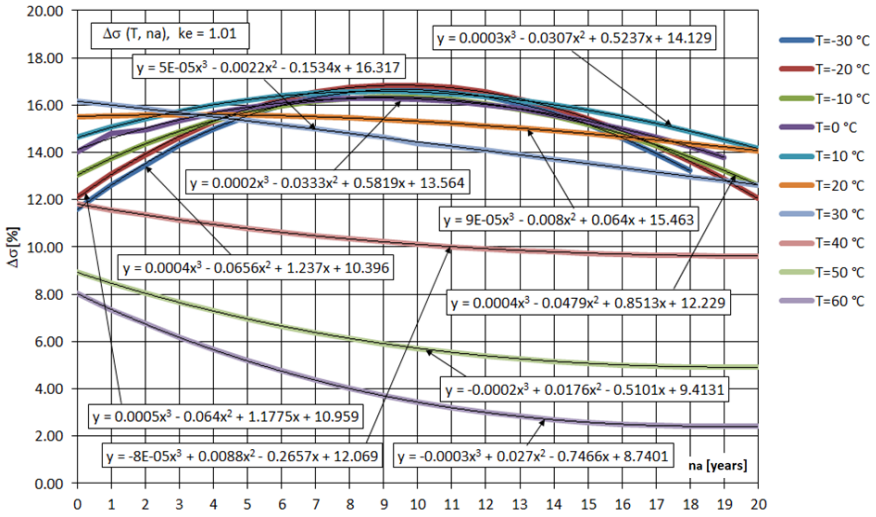

Fig. 4d. The graphs of Von Mises stress variation Δσ (n_a,T = ct.) for k_e = 1.01

For the lateral cover with ellipticity k_e = 1.02, the results are given in Table 3.

Table 3: The Von Mises stress in elliptical lateral cover with k_e = 1.02

	T [^{0}C]	-30^{0}C	-20^{0}C	-10^{0}C	0^{0}C	10^{0}C	20^{0}C	30^{0}C	40^{0}C	50^{0}C	60^{0}C
n_a [years]	s [mm]	σ [N/mm^2]									
0	9.2	668.23	642.07	616.33	591.39	568.08	547.18	532.25	520.56	509.2	516.17
1	9.08	681.00	648.51	622.83	597.85	574.07	552.53	537.56	526.02	514.61	520.7
2	8.96	672.19	655.01	629.37	604.39	580.19	558.07	542.9	531.66	520.21	525.42
3	8.84	682.03	661.54	635.93	610.95	586.42	563.82	548.47	537.5	526	530.33
4	8.72	689.20	668.1	642.53	617.54	592.76	569.78	554.25	543.52	531.98	535.43
5	8.6	697.88	674.69	649.15	624.16	599.22	575.94	560.26	549.73	538.16	540.73
6	8.48	704.22	681.31	655.8	630.81	605.79	582.31	566.5	556.13	544.53	546.12
7	8.36	709.74	687.95	662.48	637.49	612.48	588.88	572.96	562.72	551.09	551.89
8	8.24	0	694.63	669.19	644.2	619.28	595.66	579.64	569.49	557.85	557.75
9	8.12	0	701.34	675.92	650.94	626.2	602.65	586.55	576.45	564.8	563.81
10	8	0	708.07	682.68	657.72	633.23	609.82	593.7	581.52	571.87	570.09
11	7.88	0	0	689.47	664.51	640.38	617.23	601.03	590.93	579.28	576.5
12	7.76	0	0	696.29	671.34	647.64	624.84	608.61	598.45	586.81	583.14
13	7.64	0	0	703.14	678.19	655.02	632.65	616.41	606.16	594.53	589.96
14	7.52	0	0	0	685.08	662.51	640.66	624.43	614.06	602.45	596.98

15	7.4	0	0	0	692.00	670.12	648.88	632.68	622.14	610.56	604.18
16	7.28	0	0	0	698.95	677.84	657.31	641.15	630.41	618.86	611.58
17	7.16	0	0	0	705.93	685.67	665.94	649.85	638.87	627.36	619.17
18	7.04	0	0	0	0	693.62	674.78	658.77	647.52	636.05	626.95
19	6.92	0	0	0	0	701.69	683.83	667.91	656.35	644.93	634.93
20	6.8	0	0	0	0	709.9	693.17	677.24	665.36	653.95	642.57

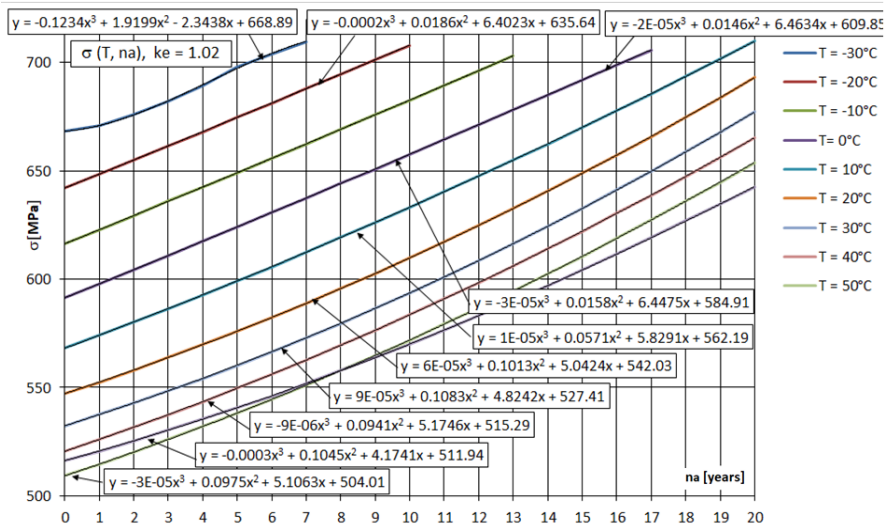

Fig. 5a. The graphs of Von Mises stress σ (n_a,T = ct.) for k_e = 1.02

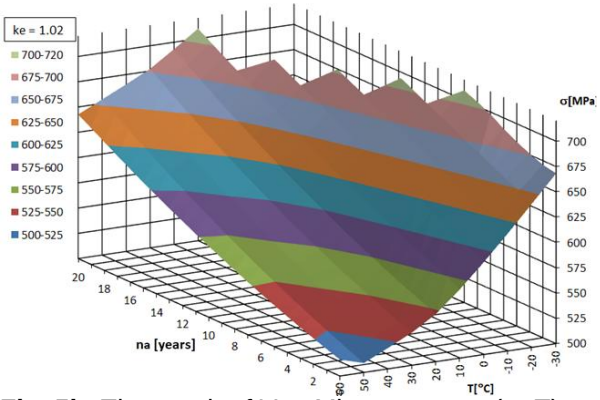

Fig. 5b. The graph of Von Mises stress σ (n_a,T) for k_e = 1.02

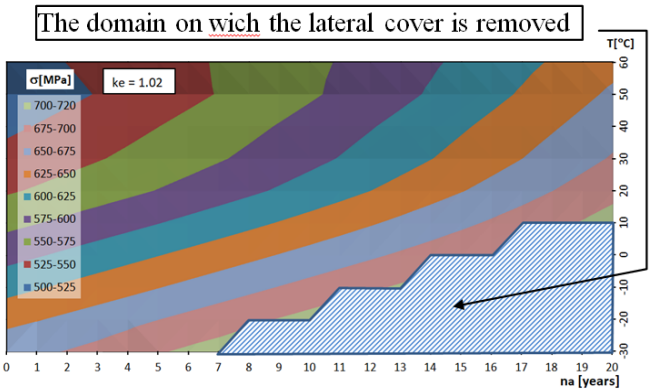

Fig. 5c. The graph in top view of Von Mises stress σ (n_a,T) for k_e = 1.02

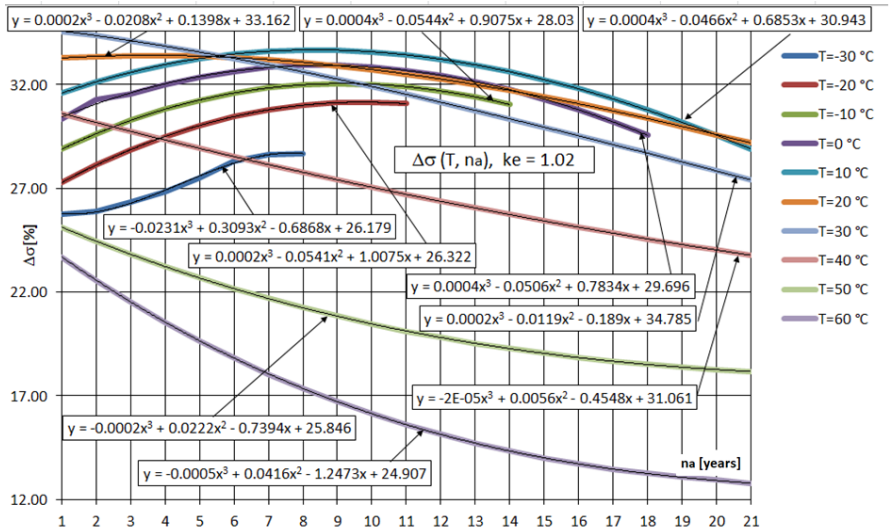

Fig. 5d. The graphs of Von Mises stress variation Δσ (n_a,T = ct.) for k_e = 1.02

For the lateral cover with ellipticity k_e = 1.03, the results are given in Table 4.

Table 4: The Von Mises stress in elliptical lateral cover with k_e = 1.03

	T [^{0}C]	-30^{0}C	-20^{0}C	-10^{0}C	0^{0}C	10^{0}C	20^{0}C	30^{0}C	40^{0}C	50^{0}C	60^{0}C
n_a [years]	s [mm]	σ [N/mm^2]									
0	9.2	0	0	692.9	668.61	645.46	623.8	608.63	599.48	590.57	581.97
1	9.08	0	0	700.5	675.92	652.38	630.36	614.74	605.08	595.77	586.73
2	8.96	0	0	708.05	683.22	659.33	636.99	620.98	610.89	601.17	591.75
3	8.84	0	0	0	690.51	666.31	643.72	627.38	616.88	606.8	597.03
4	8.72	0	0	0	697.78	673.33	650.53	633.93	623.07	612.65	602.56
5	8.6	0	0	0	705.03	680.38	657.44	640.63	629.45	618.72	608.34
6	8.48	0	0	0	0	687.46	664.44	647.48	636.02	625.01	614.37
7	8.36	0	0	0	0	694.57	671.54	654.49	642.78	631.53	620.66
8	8.24	0	0	0	0	701.72	678.72	661.66	649.73	638.27	627.2
9	8.12	0	0	0	0	708.9	686	668.97	656.87	645.23	633.99
10	8	0	0	0	0	0	693.35	676.43	664.2	652.42	641.02
11	7.88	0	0	0	0	0	700.83	684.07	671.72	659.83	648.33
12	7.76	0	0	0	0	0	708.38	691.85	679.43	667.46	655.87
13	7.64	0	0	0	0	0	0	699.78	687.33	675.32	663.67
14	7.52	0	0	0	0	0	0	707.86	695.42	683.39	671.73
15	7.4	0	0	0	0	0	0	0	703.7	691.69	680.03
16	7.28	0	0	0	0	0	0	0	0	700.22	688.59
17	7.16	0	0	0	0	0	0	0	0	708.96	697.39
18	7.04	0	0	0	0	0	0	0	0	0	706.45

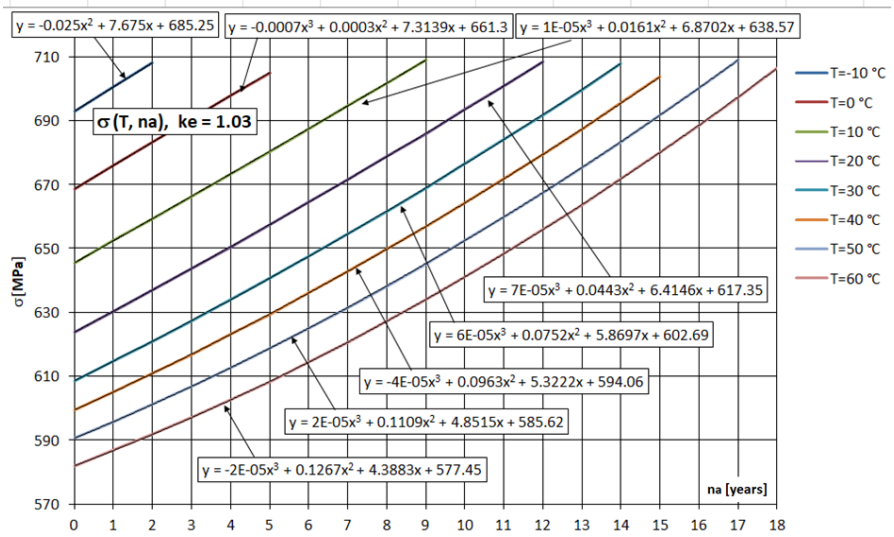

Fig. 6a. The graphs of Von Mises stress σ (n_a,T = ct.) for k_e = 1.03

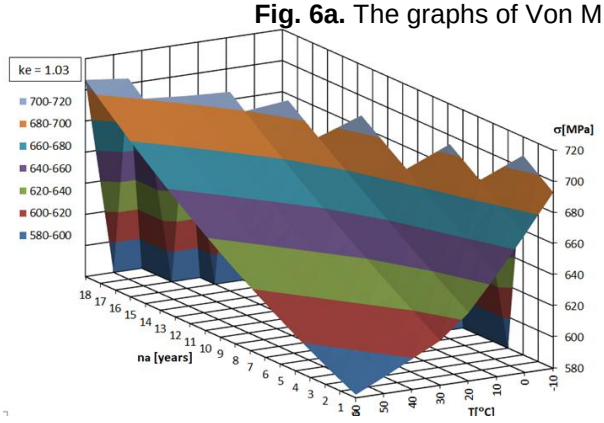

Fig. 6b. The graphs of Von Mises stress σ (n_a,T) for k_e = 1.03

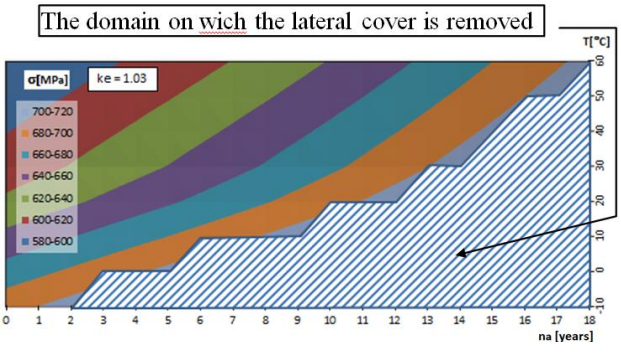

Fig. 6c. The graphs in top view of Von Mises stress σ (n_a,T) for k_e = 1.03

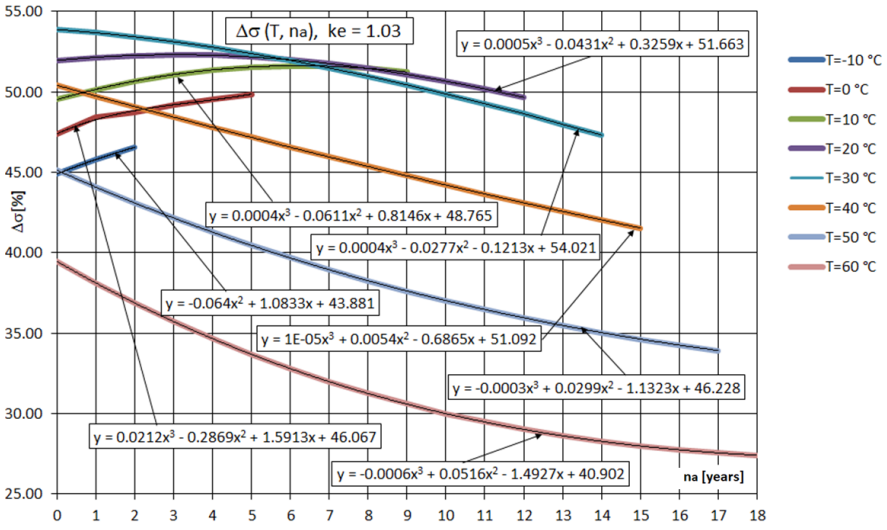

Fig. 6d. The graphs of Von Mises stress variation $\Delta\sigma$ (n_a,T = ct.) for k_e = 1.03

For lateral cover with ellipticity k_e = 1.04, the results are given in Table 5.

Table 5: The Von Mises stress in elliptical lateral cover with k_e = 1.04

	T [^{0}C]	-30^{0}C	-20^{0}C	-10^{0}C	0^{0}C	10^{0}C	20^{0}C	30^{0}C	40^{0}C	50^{0}C	60^{0}C
n_a [years]	s [mm]	σ [N/mm^2]									
0	9.2	0	0	0	0	0	704.51	687.54	676.32	665.62	655.22
1	9.08	0	0	0	0	0	0	694.75	683.23	672.46	662.02
2	8.96	0	0	0	0	0	0	702	690.26	679.4	668.95
3	8.84	0	0	0	0	0	0	709.3	697.37	686.45	675.98
4	8.72	0	0	0	0	0	0	0	704.58	693.61	683.14
5	8.6	0	0	0	0	0	0	0	0	700.87	690.41
6	8.48	0	0	0	0	0	0	0	0	708.24	697.79
7	8.36	0	0	0	0	0	0	0	0	0	705.28

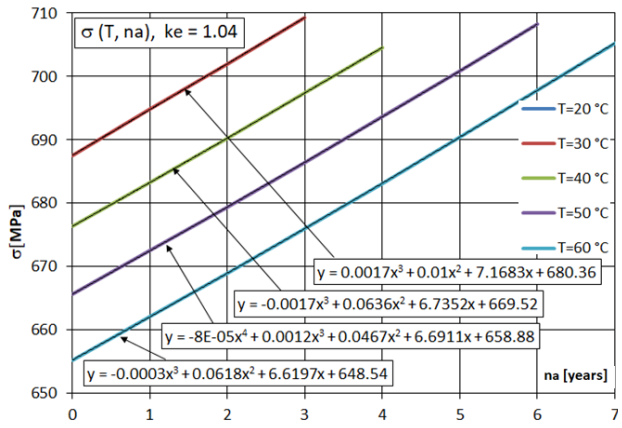

Fig. 7a. The graphs of Von Mises stress σ (n_a,T = ct.) for k_e = 1.04

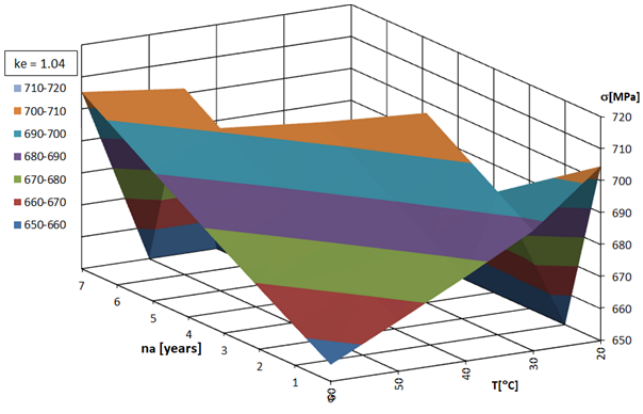

Fig. 7b. The graphs of Von Mises stress σ (n_a,T) for k_e = 1.04

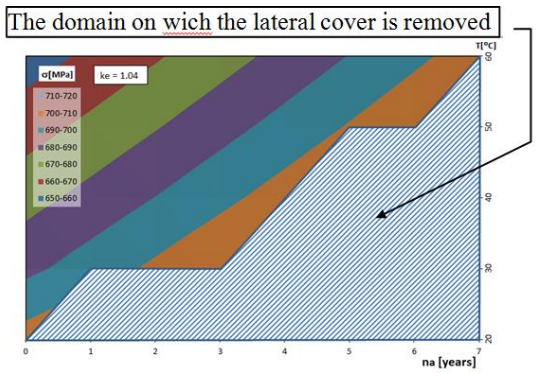

Fig. 7c. The graphs in top view of Von Mises stress for k_e = 1.04

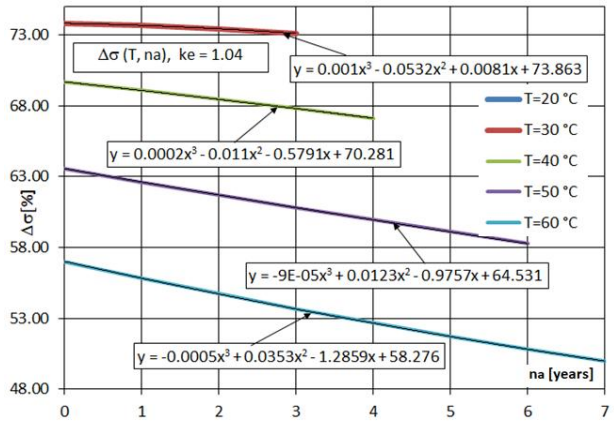

Fig. 7d. The graphs of Von Mises stress variation $\Delta\sigma$ (n_a,T = ct.), σ (n_a,T) for k_e = 1.04

4. Discussion

In the elliptical deformation state for k_e = 1.01, the semi-axes of the ellipse have deviations from the radius of undeformed circular cover of: Δa, Δb < 0.49 %, producing the following overlapped effects over the corrosion effect:

- the stress state is comprised between the minimum value of σ = 443.5 MPa at T = 50 ^{0}C and n_a = 0 years and the maximum value of σ = 705.41 MPa at T = -30 ^{0}C and n_a = 18 years, (Table 1).
- at the same time in Table 1 it can be seen that for T = -30 ^{0}C, the cover totally loses the capacity to resist to stress coming out of use after n_a = 18 years of exploitation.
- the stress state increases from $\Delta\sigma$ = 2.41 % at T = 60 ^{0}C, for n_a = 20 years, to $\Delta\sigma$ = 16.84 % for T = -20 ^{0}C, for n_a = 10 years, (as shown in Figure 4d) they touch maximum growth values over $\Delta\sigma$ > 16 %, for n_a = 4 years up to n_a =14 years and temperatures between T = -30 ^{0}C up to T = 10 ^{0}C, (as shown in Table 2 and Figure 4d).
- overall exploitation time is reduced by 1 % of imposed design time.

At the elliptic deformation state for k_e = 1.02, the semi-axes have the deviation: Δa, Δb < 0.99 %.

- the exploitation time is reduced by 16.5% over the total exploitation time, especially at the negative temperatures where we have for T = -30 °C / -20°C / -10 °C and 0 °C, large diminutions of: 65 % / 50 % / 35 % and 15 %, respectively.
- the minimum stress is σ = 509.2 MPa at T = 50 ^{0}C and n_a = 0 years and maximum of σ = 709.74 MPa at T = -30 ^{0}C and n_a = 7 years, (as shown in Table 3 and Figure 5a).
- the stress state increases between $\Delta\sigma$ = 12.76% at T = 60^{0}C, for n_a = 20 years, up to $\Delta\sigma$ = 34.56 % at T = 30 ^{0}C, for n_a = 0 years, (as shown in Fig. 5d) growing maximum $\Delta\sigma$ > 34%, for n_a = 0 year up to n_a = 2 years and T = 30 ^{0}C, (as shown in Table 3 and Figure 5d).

At the elliptic deflection state for k_e = 1.03, the semi-axes have deviations of: Δa, Δb < 1.48 %.

- overall exploitation time is greatly diminished throughout the operating temperature range, becoming 54.5 % of the total time; at negative temperatures of: T = -30 °C and T = -20 °C, the reduction is complete and then continued at: T / -10 °C / 0 °C / 10 °C / 20 °C / 30 °C / 40 °C / 50 °C / 60 °C with decreased values by: 75 % / 55 % / 40 % / 30 % / 25 % / 15 % and 10 %.
- the minimum effort is σ = 581.97.2 MPa at T = 60 ^{0}C and n_a = 0 years and maximum σ = 708.96 MPa at T = 50 ^{0}C and n_a = 17 years, (as shown in Table 4 and Figure 6a).
- the state of stress increases between $\Delta\sigma$ = 27.42 % at T = 60 ^{0}C, for n_a = 18 years, to $\Delta\sigma$ = 53.87 % at T = 30 ^{0}C, for n_a = 0 years, (as shown in Figure 6d) growing maximum $\Delta\sigma$ > 53 %, for n_a = 0 years up to n_a = 3 years and T = 30 ^{0}C, (as shown in Table 4 and Figure 6d).

At the elliptic deflection state for k_e = 1.04, the semi-axes of the ellipse have deviations of: Δa, Δb < 1.97 %.

- the overall exploitation time is drastically reduced over the entire temperature range to 87.5 % of the total exploitation time, especially at temperatures between T = -30 °C to T = 10 °C for: T = 20 °C, 60 °C and regressive, at the temperatures of: T / 20 °C / 30 °C / 40 °C / 50 °C / and 60 °C, we have diminutions of: 95 % / 85 %/ 80 % and 70 %.

- the minimum stress is σ = 655.22 MPa at T = 60 ^{0}C and n_a = 0 years and maximum σ = 709.30 MPa at T = 30 ^{0}C and n_a = 3 years, (as shown in Table 5).
- the stress state increases from $\Delta\sigma$ = 27.42 % to T = 60 ^{0}C, for n_a = 18 years, to $\Delta\sigma$ = 73.82 % at T = 30 ^{0}C, for n_a = 0 years, (as shown in Fig. 6d) maximum growth values $\Delta\sigma$ > 73 %, for n_a = 0 years up to n_a = 2 years and T = 30 ^{0}C, (as shown in Table 5 and Figure 7d).

The final conclusion is that ellipticity has a major influence on the state of stress and the exploitation period (which corresponds to the time of premature elimination from use of the cover) for ellipticity with k_e = 1.01 the stress state increases to $\Delta\sigma$ = 16.84 % with a modest decrease in exploitation time < 1%, but increasing this ellipticity to: k_e = 1.02 / k_e = 1.03 and k_e = 1.04, the state of stress increases greatly with: $\Delta\sigma$ = 34.56 % / $\Delta\sigma$ = 53.87 %, respectively $\Delta\sigma$ = 73.82 %, decreasing the total or partial exploitation time by: 16.5 %, 54.5 % and 87.5 %; for the ellipticity k_e = 1.03, the exploitation time is reduced to n_a = 18 years, while for k_e = 1.04 the exploitation time is reduced at n_a = 7 years.

5. Conclusions

This study shows the influence on the Von Mises effort state by modification of the cylindrical shape to an elliptical shape of a lateral pressurized cylindrical fuel tank.
It can be concluded that at low values of coefficient of ellipticity k_e the increase in elliptical cover efforts is very important.
At negative temperatures with increasing the ellipticity coefficient, Von Mises stresses are much higher than in the case of positive temperature stresses produced by the same deformation state.
The influence of the shape deviation of the lateral shell of the tank generates efforts that overlap with the efforts of the variation of temperature, corrosion and loading pressure.
The limitation of the exploitation period by removal from use to exceed the permissible effort is strongly influenced by the deviation of the shape from the circularity through the elliptical form compared to the initial cylindrical cover at which the pressurized fuel tank was designed.

Financial disclosure: Neither author has a financial or proprietary interest in any material or method mentioned.
Competing interests: The authors declare that they have no significant competing financial, professional or personal interests that might have influenced the performance or presentation of the work described in this manuscript.

References

[1] A.C. Nedelcu, "Romanian automotive industry – analysis made from the intellectual capital perspective", Revista Economica, vol. 67, no. 5, pp. 80-89, 2015;
[2] A. Hagiu, M. Platis, "The evolution of the Romanian car industry and its position on European market", STUDIA UBB NEGOTIA, vol. 57 (LVII), 2, pp. 65 - 91, 2012;
[3] A. Misztal, N. Belu, N. Rachieru, "Comparative Analysis of Awareness and Knowledge of APQP Requirements in Polish and Romanian Automotive Industry", Applied Mechanics and Materials, vol. 657, pp. 981-985, 2014;
[4] G. Matache, C. Cristescu, C. Dumitrescu, V. Miroiu, "Pregătirea specialiștilor în vederea adaptabilității și creșterii competitivității", Magazine of Hydraulics, Pneumatics, Tribology, Ecology, Sensorics, Mechatronics (HIDRAULICA), no. 3-4, pp. 7-14, 2012. ISSN 1453-7303;
[5] E. Lisowski, W. Czyzycki, "Transport and storage of LNG in container tanks", Journal of KONES Powertrain and Transport, vol. 18, no. 3, pp. 193-201, 2011;
[6] Chen Shr-Hung, "Novel design and optimization of vehicle's natural gas fuel tank". Master's Thesis presented to the Faculty of the College of the Engineering and Technology, Ohio University, March 1997;
[7] M.C. Ghiţă, A.C. Micu, M. Ţălu, Ş. Ţălu, E. Adam, "Computer-Aided Design of a classical cylinder gas tank for the automotive industry", Annals of Faculty of Engineering Hunedoara - International Journal of Engineering, Hunedoara, Tome XI, Fascicule 4, pp. 59-64, 2013;
[8] M.C. Ghiţă, A.C. Micu, M. Ţălu, Ş. Ţălu, "Shape optimization of vehicle's methane gas tank", Annals of Faculty of Engineering Hunedoara - International Journal of Engineering, Hunedoara, Tome X, Fascicule 3, pp. 259-266, 2012;

[9] M.C. Ghiţă, A.C. Micu, M. Ţălu, Ş. Ţălu, "3D modelling of a shrink fitted concave ended cylindrical tank for automotive industry". Acta Technica Corviniensis – Bulletin of Engineering, Hunedoara, Romania, Tome VI, Fascicule 4, pp. 87-92, 2013;
[10] M.C. Ghiţă, A.C. Micu, M. Ţălu, Ş. Ţălu, "3D modelling of a gas tank with reversed end up covers for automotive industry", Annals of Faculty of Engineering Hunedoara - International Journal of Engineering, Hunedoara, Tome XI, Fascicule 3, 2013, pp. 195-200, 2013;
[11] M.C. Ghiţă, C.Ş. Ghiță, Ş. Ţălu, S. Rotaru, "Optimal design of cylindrical rings used for the shrinkage of vehicle tanks for compressed natural gas", Annals of Faculty of Engineering Hunedoara - International Journal of Engineering, Hunedoara, Tome XII, Fascicule 3, pp. 243-250, 2014;
[12] M.C. Ghiţă, A.C. Micu, M. Ţălu, Ş. Ţălu, "Shape optimization of a thoroidal methane gas tank for automotive industry", Annals of Faculty of Engineering Hunedoara - International Journal of Engineering, Hunedoara, Tome X, Fascicule 3, pp. 295-297, 2012;
[13] M.V.J. Bhavana, Rao S. Janardhana, B A.N. Murthy, "Design and analysis of horizontal LPG storage pressure vessel for variable dimensional constraints under given physical parameters", International Journal & Magazine of Engineering, Technology, Management and Research, vol. 4, issue 5, pp. 342 - 351, 2017;
[14] M. Ziółkowska, D. Wardzińska, "Corrosiveness of fuels during storage processes", published by IntechOpen. http://dx.doi.org/10.5772/59803;
[15] P. Mould, T. Burton, R. Daley, S. Itonaga, T. Kikuchi, S. Jokela, M. Luciani, M. McCosby, D. Paul, T. Sakiyama, G. Schwerzel, R. Sheffield, G. Tarrance, W. Warnecke, "Evaluation of the corrosion durability of steel systems for automobile fuel tanks," SAE Technical Paper 2005-01-0540, 2005, https://doi.org/10.4271/2005-01-0540;
[16] P.P. Deshpande, "Structural analysis of integration of a non-cylindrical CNG fuel tank", Master's report, Michigan Technological University, 2015. https://digitalcommons.mtu.edu/etds/988;
[17] Ş. Ţălu, "Geometrie descriptivă" (Descriptive geometry), Cluj-Napoca, Risoprint Publishing house, 2010;
[18] A. Florescu-Gligore, Ş. Ţălu, D. Noveanu, "Reprezentarea şi vizualizarea formelor geometrice în desenul industrial" (Representation and visualization of geometric shapes in industrial drawing), Cluj-Napoca, U. T. Pres Publishing house, 2006;
[19] A. Florescu-Gligore, M. Orban, Ş. Ţălu, "Cotarea în proiectarea constructivă şi tehnologică" (Dimensioning in technological and constructive engineering graphics), Cluj-Napoca, Lithography of The Technical University of Cluj-Napoca, 1998;
[20] C. Racocea, Ş. Ţălu, "Reprezentarea formelor geometrice tehnice în axonometrie" (The axonometric representation of technical geometric shapes), Cluj-Napoca, Napoca Star Publishing house, 2011;
[21] Ş. Ţălu, C. Racocea, "Reprezentări axonometrice cu aplicaţii în tehnică" (Axonometric representations with applications in technique), Cluj-Napoca, MEGA Publishing house, 2007;
[22] Carlos Martines Ortiz, "2D and 3D shape descriptors". Thesis for the degree of Doctor of Philosophy in Computer Science, University of Exeter, GBR, 2010;
[23] Ş. Ţălu, M. Ţălu, "CAD generating of 3D supershapes in different coordinate systems", Annals of Faculty of Engineering Hunedoara - International Journal of Engineering, Hunedoara, Tome VIII, Fascicule 3, pp. 215-219, 2010;
[24] Ş. Ţălu, M. Ţălu, "A CAD study on generating of 2D supershapes in different coordinate systems", Annals of Faculty of Engineering Hunedoara - International Journal of Engineering, Hunedoara, Tome VIII, Fascicule 3, pp. 201-203, 2010;
[25] Ş. Ţălu, "CAD representations of 3D shapes with superellipsoids and convex polyhedrons", Annals of Faculty of Engineering Hunedoara - International Journal of Engineering, Hunedoara, Tome IX, Fascicule 3, 2011, pp. 349-352, 2011;
[26] Ş. Ţălu, "Study on the construction of complex 3D shapes with superellipsoids and supertoroids", Annals of Faculty of Engineering Hunedoara - International Journal of Engineering, Hunedoara, Tome IX, Fascicule 3, pp. 299-302, 2011;
[27] Ş. Ţălu, "Complex 3D shapes with superellipsoids, supertoroids and convex polyhedrons", Journal of Engineering Studies and Research, Bacău, vol. 17, no. 4, pp. 96-100, 2011;
[28] Ş. Ţălu, "Generation of 3D shapes with superellipsoids, supertoroids, super cylinders and super cones", Journal of Engineering Studies and Research, Bacău, vol. 18, no. 2, pp. 135-139, 2012;
[29] Ş. Ţălu, "Grafică tehnică asistată de calculator" (Computer assisted technical graphics), Cluj-Napoca, Victor Melenti Publishing house, 2001;
[30] Ş. Ţălu, "Reprezentări grafice asistate de calculator" (Computer assisted graphical representations), Cluj-Napoca, Osama Publishing house, 2001;
[31] Ş. Ţălu, "Limbajul de programare AutoLISP. Teorie şi aplicaţii", (AutoLISP programming language. Theory and applications), Cluj-Napoca, Risoprint Publishing house, 2001;
[32] Ş. Ţălu, "AutoCAD 2005", Cluj-Napoca, Risoprint Publishing house, 2005;

[33] Ş. Ţălu, M. Ţălu, “AutoCAD 2006. Proiectare tridimensională“ (AutoCAD 2006. Three-dimensional designing), Cluj-Napoca, MEGA Publishing house, 2007;
[34] Ş. Ţălu, “AutoCAD 2017“, Cluj-Napoca, Napoca Star Publishing house, 2017;
[35] C. Bîrleanu, Ş. Ţălu, “Organe de maşini. Proiectare şi reprezentare grafică asistată de calculator“ (Machine elements. Designing and computer assisted graphical representations), Cluj-Napoca, Victor Melenti Publishing house, 2001;
[36] T. Niţulescu, Ş. Ţălu, “Aplicaţii ale geometriei descriptive şi graficii asistate de calculator în desenul industrial“ (Applications of descriptive geometry and computer aided design in engineering graphics), Cluj-Napoca, Risoprint Publishing house, 2001;
[37] Ş. Ţălu, “Micro and nanoscale characterization of three dimensional surfaces. Basics and applications”, Napoca Star Publishing House, Cluj-Napoca, Romania, 2015;
[38] M. Rusănescu, "Material requirements planning, inventory control system in industry", Magazine of Hydraulics, Pneumatics, Tribology, Ecology, Sensorics, Mechatronics (HIDRAULICA), no. 1, pp. 21-25, 2014. ISSN 1453-7303;
[39] M. Țălu, “Calculul pierderilor de presiune distribuite în conducte hidraulice” (Calculation of distributed pressure loss in hydraulic pipelines), Craiova, Universitaria Publishing house, 2016;
[40] M. Țălu, “Pierderi de presiune hidraulică în conducte tehnice cu secțiune inelară. Calcul numeric și analiză C.F.D.” (Hydraulic pressure loss in technical piping with annular section. Numerical calculation and C.F.D.), Craiova, Universitaria Publishing house, 2016;
[41] M. Ţălu, “Mecanica fluidelor. Curgeri laminare monodimensionale” (Fluid mechanics. The monodimensional laminar flow), Craiova, Universitaria Publishing house, 2016;
[42] M. Ţălu, "The influence of the corrosion and temperature on the Von Mises stress in the lateral cover of a pressurized fuel tank", Magazine of Hydraulics, Pneumatics, Tribology, Ecology, Sensorics, Mechatronics (HIDRAULICA), no. 4, pp. 89-97, 2017, ISSN 1453-7303;
[43] D. Vintilă, M. Ţălu, Ş. Ţălu, “The CAD analyses of a torospheric head cover of a pressurized cylindrical fuel tank after the crash test”, Magazine of Hydraulics, Pneumatics, Tribology, Ecology, Sensorics, Mechatronics (HIDRAULICA), no. 4, pp. 57-66, 2017, ISSN 1453-7303;
[44] M. Bică, M. Ţălu, Ş. Ţălu, “Optimal shapes of the cylindrical pressurized fuel tanks”, Magazine of Hydraulics, Pneumatics, Tribology, Ecology, Sensorics, Mechatronics (HIDRAULICA), no. 4, pp. 6-17, 2017. ISSN 1453-7303;
[45] *** Autodesk AutoCAD 2017 software;
[46] *** SolidWorks 2017 software;
[47] *** Microsoft Excel 2017 software;
[48] *** Maple 2016 software.